X-ray absorption study of molten yttrium trihalides

Y. Okamoto,[a]* M. Akabori,[a] H. Motohashi,[b] H. Shiwaku[c] and T. Ogawa[a]

[a]Department of Materials Science, Japan Atomic Energy Research Institute, Tokai-mura, Naka-gun, Ibaraki-ken 319-1195, Japan, [b]SPring-8 Service Corporation, Kouto, Mikazuki-cho, Sayo-gun, Hyogo-ken 678-1205, Japan, and [c]Synchrotron Radiation Research Center, Japan Atomic Energy Research Institute, Kouto, Mikazuki-cho, Hyogo-ken 679-5143, Japan. E-mail: okamoto@molten.tokai.jaeri.go.jp

The local structure and structural changes in molten YCl_3–LiCl–KCl and molten YBr_3–LiBr systems have been investigated by using a high-temperature extended X-ray absorption fine structure (EXAFS) technique. The behaviour of octahedral coordination of the halide ion (Cl^- and Br^-) around the Y^{3+} ion has been studied by EXAFS of the Y *K*-absorption edge. The nearest Y^{3+}—Cl^- and Y^{3+}—Br^- distances and coordination numbers of halide ions around the Y^{3+} ion do not change by mixing with the alkali halides. The stabilization of the $(YCl_6)^{3-}$ and $(YBr_6)^{3-}$ octahedral coordination by adding alkali halides was suggested by decreasing the Debye–Waller factor and the anharmonicity in the nearest Y^{3+}–Cl^- and Y^{3+}–Br^- interactions. The bridging structure of the $(YBr_6)^{3-}$ octahedra sharing a Br^- ion in the molten YBr_3–LiBr system was studied by EXAFS of the Br *K*-absorption edge. The coordination number of Y^{3+} around the Br^- ion decreases from 2 in the pure melt to almost 1 in the 30mol% and 15mol% YBr_3 melts. This suggests that the bridging is almost broken and the stable octahedron exists freely in the LiBr-rich melts.

Keywords: XAFS; molten salts; high temperature; rare-earth halides; halides; mixing.

1. Introduction

Considerable information on the structure of molten rare-earth halides has been reported by using X-ray diffraction (XRD) (Mochinaga *et al.*, 1991; Okamoto *et al.*, 1999, 2000; Okamoto & Ogawa, 1999*a*), neutron diffraction (ND) (Saboungi *et al.*, 1991; Wasse & Salmon, 1999*a*,*b*,*c*; Wasse *et al.*, 2000), Raman spectroscopy (Papatheodorou, 1975, 1977; Dracopoulos *et al.*, 1997; Photiadis *et al.*, 1998) and molecular dynamics (MD) techniques (Abramo & Caccamo, 1994; Okamoto *et al.*, 1996; Sakurai *et al.*, 1998; Takagi *et al.*, 1999; Hutchinson *et al.*, 1999). To sum up the major characteristics of the structure for the pure trihalide melts:

(i) Octahedral coordination $(MX_6)^{3-}$, in which a rare-earth ion is surrounded by six halide ions as shown in Fig. 1(*a*), is a predominant species in most systems.

(ii) There is a medium-ranged structural order (MRO) generated by bridging the octahedra (Figs. 1*b* and 1*c*). The bridging is formed by sharing a Br^- ion between the octahedra. A first sharp diffraction peak (FSDP) observed in the diffraction studies is thought to be proof that MRO exists in the melt.

Papatheodorou (1975, 1977) discovered the existence of the octahedral coordination for the first time using Raman spectra of molten YCl_3 and $LaCl_3$. He detected Raman active modes corresponding to $(MX_6)^{3-}$ octahedra in molten YCl_3 with alkali chlorides. In addition, he suggested that the octahedra must be distorted in the YCl_3-rich composition. The presence of the octahedral coordination was also confirmed by X-ray and neutron diffraction. Mochinaga *et al.* (1991) reported from systematic XRD measurements that the coordination number of Cl^- ions around cations is about 6 in many molten rare-earth trichlorides. Saboungi *et al.* (1991) reported the existence of the $(YCl_6)^{3-}$ octahedron and a FSDP suggesting MRO around Q = 0.95 Å^{-1} in the pulse neutron diffraction analysis of molten YCl_3. Recently, systematic ND results of molten rare-earth halides were reported by Wasse & Salmon (1999*a*,*b*,*c*). They showed that the structure of molten rare-earth trihalides can be expressed by scaling of halide ions from data analysis based on the difference function method. This means, for example, that the structures of molten $LaCl_3$, $LaBr_3$ and LaI_3 are isomorphoric. In MD simulations, some works (Abramo & Caccamo, 1994; Okamoto *et al.*, 1996; Sakurai *et al.*, 1998) using the traditional rigid ionic model (RIM) were reported to reproduce the structure and physical properties. It was found that the structures of the molten trihalides were more precisely reproduced by the MD simulation with the polarizable ionic model (PIM) (Hutchinson *et al.*, 1999) than by MD with the RIM. Recently, Takagi *et al.* (1999) obtained partial structure factors of molten $DyCl_3$ by ND measurement with an isotopic substitution technique. They reported that the bridging of the $(DyCl_6)^{3-}$ octahedra is based on edge-sharing

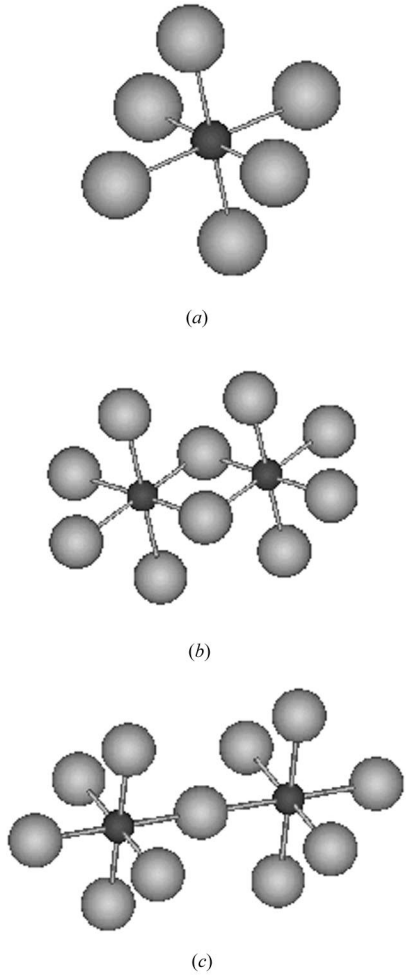

Figure 1
Models of local structures for molten rare-earth trihalides. (*a*) Octahedral coordination $(MX_6)^{3-}$. (*b*) Edge-sharing model. (*c*) Corner-sharing model. Small ball – metal ion M^{3+}. Large ball – halide ion X^-.

Dy–Cl–Dy clusters (Fig. 1*b*). The partial structure factors of the Dy–Dy correlation were nicely reproduced by the MD simulation with the PIM model. Further detailed and new information from the EXAFS measurements are expected to develop the structural analysis of molten trihalides.

The EXAFS technique is a relatively new experimental tool in the field of study of molten salts, though many results have been reported for solid catalysts, solutions, amorphous solids *etc.* The application of the EXAFS technique to the study of molten salts produces some experimental difficulties. In EXAFS measurements using transmission techniques we have to create and keep a thin liquid film at high temperatures. Di Cicco *et al.* (1996, 1997) reported EXAFS studies of molten alkali bromides. They used a pellet of boron nitride containing a dispersion of alkali halide. The EXAFS measurement was performed under the condition where the sample was molten with the solid boron nitride matrix. Ablanov *et al.* (1999) used a specially designed quartz cell for the measurement of molten $PbCl_2$. In any case, the above devices are necessary for the design of the sample container in the measurements of molten salt systems. Information concerning local structure, *i.e.* interionic distance, coordination number, and fluctuation and vibration of the interaction around selected ion species, is expected from an EXAFS analysis of a molten salt. Using the diffraction method, it is very difficult to detect the distortion of the $(MX_6)^{3-}$ octahedron suggested by Raman studies. Raman spectroscopy may be a better technique than the diffraction method in the elucidation of the local structure; however, direct information, such as interionic distance, is not obtained using Raman spectroscopy. Thus the EXAFS technique has advantages over both diffraction and Raman spectroscopy. We have already reported the EXAFS of the Br *K*-absorption edge in molten $LaBr_3$ (Okamoto *et al.*, 2000). In the analysis it was concluded that most Br^- ions are connected to two La^{3+} ions in the form of corner-sharing. We have reported (Okamoto *et al.*, 1998, 1999; Okamoto & Ogawa, 1999*b*) that many physical properties, such as shear viscosity and mixing enthalpy of the molten rare-earth trihalides and their mixtures with alkali halides, are affected by structural changes of the octahedral coordination and the bridging of the octahedron. In the present work, systematic EXAFS measurements of molten YCl_3 and YBr_3 with alkali halides have been performed in order to investigate the behaviour of the coordination of halide ions around Y^{3+} ions and the bridging.

2. Experimental

2.1. *Sample preparation*

All samples were handled in a purified argon atmosphere (less than 2 p.p.m. oxygen and 343 K dew point). The samples YCl_3 (99.9% purity, Aldrich) and YBr_3 (99.9% purity, Aldrich) used in the EXAFS measurement were purified using a sublimation technique. Eutectic LiCl–41%KCl (99.99% purity, APL Engineered Materials Inc.) and LiBr (99.9% purity, Aldrich) were dried under high vacuum at 473 K for 2 d. Selected compositions were 100, 50, 30 and 15% trihalides concentration for each system. Prescribed powder mixtures of YCl_3–LiCl–KCl and YBr_3–LiBr systems were melted in a closed quartz vessel and cooled rapidly after mixing.

2.2. *XAFS experiment*

EXAFS measurements using transmission techniques were performed at beamline BL27B (X-rays ranging from 5 to 20 keV) of the Photon Factory in the Institute of Materials Structure Science of the High Energy Accelerator Research Organization in Tsukuba, Japan. The ring energy was 2.5 GeV and the current during the experiments ranged from 250 to 400 mA. The radiation was monochromated by an Si(111) double crystal. EXAFS measurements based on the Y *K*-absorption edge (E_0 = 17.038 keV) were performed for molten YCl_3-eutectic LiCl–KCl and YBr_3–LiBr systems. In the YBr_3–LiBr system, additional EXAFS data at the Br *K*-absorption edge (E_0 = 13.474 keV) were obtained. Fixed time scans with 1 to 3 s per data point were repeated several times in the energy range from 16.5 to 18.5 keV for the Y *K*-edge and from 13 to 15 keV for the Br *K*-edge. The temperatures were 1173 K for molten pure YCl_3 [melting point 987 K (Mochinaga & Irisawa, 1974)] and 1200 K for molten YBr_3 [melting point 1185 K (Spedding & Danne, 1960)]. The temperature for molten YCl_3 is considerably higher than its melting point. The temperature depends on the thickness of the passage for melts in the quartz cell. First, we attempted to measure the EXAFS of molten YCl_3 at 1073 K by using a cell of thickness 0.1 mm. However, the melt did not pass into the narrow path, probably owing to high shear viscosity (Hayashi *et al.*, 1998). After elevating the temperature to 1173 K, we obtained the thin liquid film in the cell. The temperatures for the mixtures were 973 K for the molten YCl_3-eutectic (LiCl–KCl) system and 1200 K for the molten YBr_3–LiBr system.

A specially designed quartz cell (Okamoto *et al.*, 2000) was used in the measurement. The cell was sandglass-shaped consisting of an upper tank for the solid sample, a path of thickness 0.1 or 0.2 mm for the measurement of EXAFS, and a lower tank for dropped melts. The samples were prepared in the upper tank of the quartz cell and sealed under reduced pressure. The path through which the melt passes perpendicular to the X-ray beam was a rectangle of height 25 mm and width 5 mm. Two types of cell, having thicknesses of 0.1 and 0.2 mm, were used depending on the absorption of the samples. The cell of thickness 0.1 mm was mainly used for the pure trihalides and mixtures of 50mol% trihalides. The cell of thickness 0.2 mm was used for the 30mol% and 15mol% trihalide mixtures. The cell was placed inside an electric furnace with two small apertures for the X-ray beam. Initially it was confirmed that the XAFS $\log(I/I_0)$ spectrum formed a straight line for a blank measurement with an empty cell. Melting of the samples was recognized by a change in the transmitted X-ray intensity.

2.3. *Data analysis*

EXAFS data analysis was performed using the computer program *WinXAS* (version 1.3) developed by Ressler (1997). A Victoreen function was used for pre-edge background removal. The EXAFS signal was converted into the photoelectron wavevector k, defined as

$$k = \left[2m_e(E - E_0)/\hbar\right]^{1/2}, \tag{1}$$

where m_e is the mass of an electron and E is the energy of the incident X-ray. The parameter E_0, which is the threshold energy of the absorption edge, was defined as the maximum value of the first derivative for the edge jump in the present study. A cubic-spline fitting technique was used for extraction of the EXAFS oscillation $\chi(k)$. The EXAFS oscillation function $\chi(k)$ was Fourier-transformed to obtain the real-space information using

$$\mathrm{FT}(r) = (1/2\pi)^{1/2} \int_{k_{\min}}^{k_{\max}} k^3 \chi(k) W(k) \exp(2ikr)\, \mathrm{d}k, \tag{2}$$

where $W(k)$ is a window function for reducing termination errors in the Fourier transform. In this study, a Bessel function was used for all the systems.

The interionic distance, coordination number and Debye–Waller factor were determined by least-squares fitting. The curve fitting was

performed both in k-space and R-space. The backscattering amplitude and the phase-shift functions used in the fit were based on calculated values using the *FEFF7* code (Zabinsky *et al.*, 1995) developed at the University of Washington. In the analysis of solids at room temperature, the following equation was used in the curve fitting,

$$\chi(k) = \sum_j N_j S_j(k) F_j(k) \exp\left(-2\sigma_j^2 k^2\right) \exp\left(-2r_j/\lambda\right) \times \sin\left[2kr_j + \varphi_j(k)\right]/\left(kr_j^2\right), \quad (3)$$

where N_j is the coordination number of ion j around central ion i, $S_j(k)$ is the amplitude reduction factor mainly due to many-body effects, $F_j(k)$ is the backscattering amplitude for each neighbouring atom, σ_j is the Debye–Waller factor corresponding to thermal vibration, λ is the electron mean free path, $\varphi_{ij}(k)$ is the total phase shift experienced by a photoelectron, and r_j is the average distance of ion j from the central ion i.

It had been expected that an accurate EXAFS analysis could not be carried out for such high-temperature rare-earth trihalide melts because of the strong effect of the anharmonic vibration (Eisenberger & Brown, 1979). For example, the interatomic distance obtained for high temperatures by assuming that a peak in the Fourier transform (FT) is expressed by a Gaussian distribution function is generally shorter than that obtained by XRD analysis. According to the XAFS analysis of high-temperature Cu metal by van Hung *et al.* (1996), the nearest distance evaluated with the anharmionic contribution was different from that calculated by the harmonic model by 0.05 Å at 700 K. The peak in the FT of EXAFS spectra at high temperatures is generally asymmetric. Soldo *et al.* (1997) reported that clearly incorrect values in coordination number and Debye–Waller factor were obtained as a result of the data analysis of liquid Se when a harmonic oscillation is assumed. They had to consider the anharmonic effect beyond 923 K. The anharmonic effect was also taken into account in the present study. The following equation containing the third and the fourth cumulants proposed by Bunker (1983) was used to express effects of anharmonic vibration,

$$\chi(k) = \sum_j N_j S_j(k) F_j(k) \exp\left(-2\sigma_j^2 k^2\right) \exp\left(-r_j/\lambda\right) \exp\left(\tfrac{2}{3} C4_j k^4\right) \times \sin\left[2kr_j + \varphi_j(k) - \tfrac{4}{3} C3_j k^3\right]/\left(kr_j^2\right), \quad (4)$$

where $C3$ and $C4$ are the third and fourth cumulants. They are zero when the harmonic oscillation approximation is valid. The first cumulant corresponds to the mean value of the interionic distance. The Debye–Waller factor is equivalent to the second cumulant. The cumulant expansion method was successfully used in the high-temperature XAFS study of lead (Stern *et al.*, 1991). The agreement with the experimental XAFS data in the curve fitting was evaluated by taking a residual R, defined by

$$R = \sum_{i=1}^{N} \left|k^3\chi_{\rm exp}(k) - k^3\chi_{\rm cal}(k)\right| \Big/ \sum_{i=1}^{N} \left|k^3\chi_{\rm exp}(k)\right|. \quad (5)$$

3. Results and discussion

3.1. *Solid and molten pure melts*

Fig. 2(*a*) shows raw EXAFS oscillation functions $k^3\chi(k)$ of the Y K-edge and Fig. 2(*b*) shows their FT without correcting the phase shift for solid and molten YCl_3 and YBr_3. The range of the $\chi(k)$ data used, which is defined as $k_{\rm min}$ and $k_{\rm max}$ in equation (2), was 3.5 to 14 Å^{-1} for the solid state and 3.5 to 12 Å^{-1} for the molten state. The amplitude in the functions $k^3\chi(k)$ and the height of the first peaks in the FT corresponding to the nearest Y^{3+}–Cl^- and Y^{3+}–Br^- shells decrease after melting. The peak positions of the molten YCl_3 and YBr_3 are almost the same as those of the corresponding solids at room temperature. In the FT of the solid YCl_3, the second peak corre-

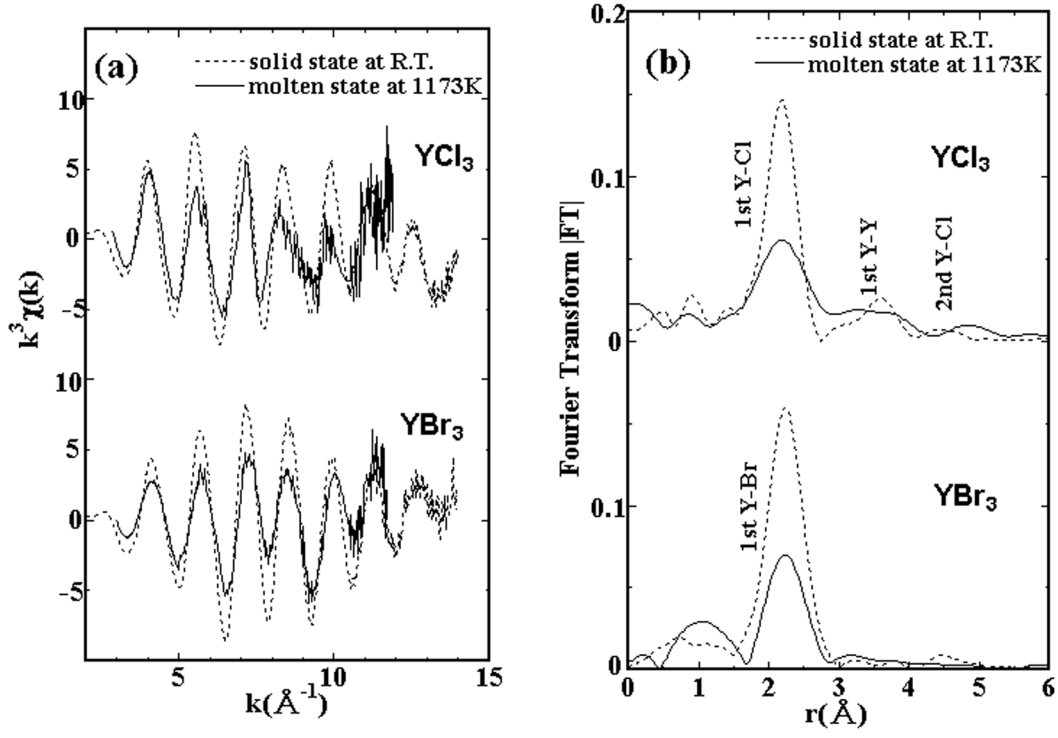

Figure 2
(*a*) Y K-edge EXAFS functions $k^3\chi(k)$ and (*b*) Fourier transforms |FT| of solid and molten YCl_3 and YBr_3.

Table 1
Structural parameters for the nearest Y^{3+}–Cl^- pair in solid and molten YCl_3 and molten YCl_3-eutectic LiCl–KCl system based on the Y *K*-absorption edge.

Coordination number N_{Cl}, interionic distance r_{Cl}, Debye–Waller factor σ^2_{Y-Cl}, third and fourth cumulants *C*3 and *C*4.

	N_{Cl}	r_{Cl} (Å)	σ^2_{Y-Cl} (Å^2)	*C*3 (10^{-3} Å)	*C*4 (10^{-4} Å)	Residual
Solid YCl_3	6.0 ± 0.1	2.65 ± 0.01	0.0063 ± 0.0004	No anharmonic effects	No anharmonic effects	6.97
Molten YCl_3	5.9 ± 0.6	2.72 ± 0.02	0.0215 ± 0.0016	0.537 ± 0.024	0.938 ± 0.047	15.70
Molten 50%YCl_3	5.9 ± 0.4	2.71 ± 0.02	0.0190 ± 0.0003	0.469 ± 0.028	0.346 ± 0.068	15.23
Molten 30%YCl_3	6.1 ± 0.4	2.69 ± 0.01	0.0149 ± 0.0009	0.295 ± 0.016	0.264 ± 0.020	16.93
Molten 15%YCl_3	6.0 ± 0.3	2.68 ± 0.03	0.0099 ± 0.0012	0.223 ± 0.025	0.068 ± 0.027	20.04

Table 2
Structural parameters for the nearest Y^{3+}–Br^- pair in solid and molten YBr_3 and molten YBr_3–LiBr system based on the Y *K*-absorption edge.

Coordination number N_{Br}, interionic distance r_{Br}, Debye–Waller factor σ^2_{Y-Br}, third and fourth cumulants *C*3 and *C*4.

	N_{Br}	r_{Br} (Å)	σ^2_{Y-Br} (Å^2)	*C*3 (10^{-3} Å)	*C*4 (10^{-4} Å)	Residual
Solid YBr_3	6.0 ± 0.1	2.82 ± 0.01	0.0135 ± 0.0004	No anharmonic effects	No anharmonic effects	8.23
Molten YBr_3	5.8 ± 0.4	2.85 ± 0.02	0.0263 ± 0.0014	0.641 ± 0.065	0.666 ± 0.025	20.39
Molten 50%YBr_3	6.1 ± 0.4	2.85 ± 0.01	0.0236 ± 0.0005	0.581 ± 0.036	0.552 ± 0.094	19.61
Molten 30%YBr_3	6.0 ± 0.4	2.84 ± 0.01	0.0171 ± 0.0013	0.388 ± 0.015	0.224 ± 0.033	27.73
Molten 15%YBr_3	6.1 ± 0.4	2.85 ± 0.01	0.0131 ± 0.0009	0.364 ± 0.008	0.250 ± 0.021	12.16

sponding to the first Y^{3+}–Y^{3+} interaction is clearer than that of YBr_3. This is simply due to the difference in the electron density of the ligands of the Y^{3+} ion. The second peak in the solid YCl_3 remains in the molten state, though becomes broader.

Fig. 3 shows *R*-space curve-fitting results of the first Y^{3+}–Cl^- interactions of solid and molten YCl_3 by using a Gaussian distribution. In the solid YCl_3, the peak is symmetric and well reproduced by a Gaussian distribution. On the other hand, the peak in the molten state is asymmetric and cannot be approximated by a single Gaussian. Similar results were confirmed in the other molten systems of this study. The following two possibilities are considered as the origin of the observed asymmetric peak: (i) overlap of two or several kinds of interactions, for example, distortion of the octahedron, or (ii) an effect of anharmonic vibration. In the neutron diffraction studies (Saboungi *et al.*, 1991; Wasse & Salmon, 1999*b*), the first Y^{3+}–Cl^- peak was successfully analyzed by using a Gaussian fitting. This means that the Y^{3+}–Cl^- interaction can be described by unique parameters (*i.e.* by a unique set of coordination number, interionic distance and displacement factor). Generally, the anharmonic vibration effect can be ignored in the radial distribution function obtained by diffraction methods. The result of the curve fitting for the molten YCl_3 assuming a single Gaussian or two kinds of Gaussians invariably resulted in 2.60 Å for the nearest Y^{3+}—Cl^- distance. This value is shorter than those in both the crystalline state (Xiang-Yun *et al.*, 1988) and the molten state (Saboungi *et al.*, 1991; Wasse & Salmon, 1999*b*). It is therefore concluded that the present EXAFS results of the molten state contain the anharmonic vibration effect. Thus the cumulant expansion method (Bunker, 1983), equation (4), was used in the curve fitting.

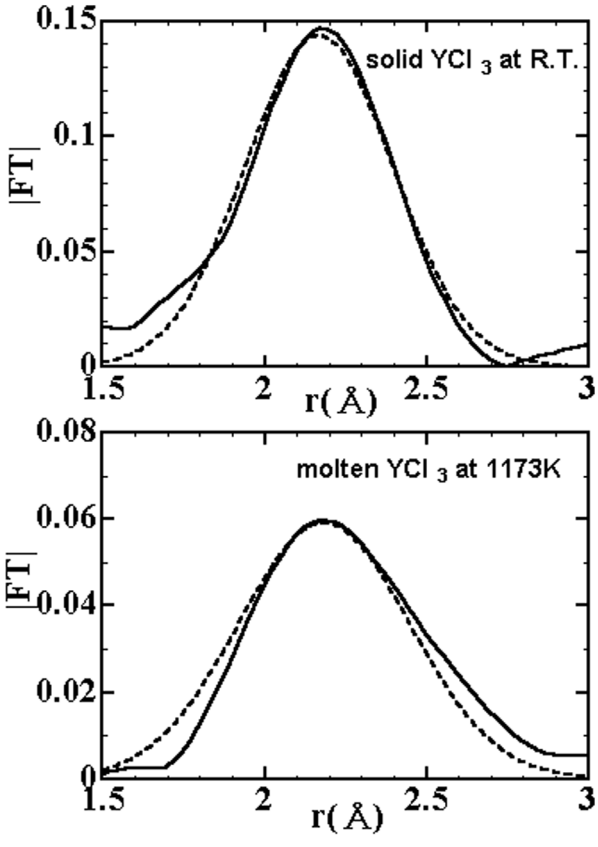

Figure 3
Fitting of the first shell using a Gaussian approximation (solid line: experimental; dashed line: fitting result).

Structural parameters such as coordination number, interionic distance and Debye–Waller factor calculated by the curve fitting are listed in Tables 1 and 2. The structural parameters of solid YCl_3 and YBr_3 are almost the same as those reported by Xiang-Yun *et al.* (1988). Crystalline YCl_3 has monoclinic structure (isomorphous with $AlCl_3$ and $DyCl_3$). Crystalline YBr_3 has a hexagonal $FeCl_3$-type structure. The nearest Y^{3+}—Cl^- and Y^{3+}—Br^- distances in the solids were 2.65 Å and 2.82 Å, respectively, in this EXAFS analysis. These values are almost the same as the values in the literature. The distance and coordination number of the nearest Y^{3+}–Cl^- interaction in molten YCl_3 were 2.72 Å and 5.9, respectively. These values are in good agreement with the results of neutron diffraction, 2.71 Å and 5.9 by Saboungi *et al.* (1991) and 2.72 Å and 5.7 by Wasse & Salmon (1999*b*). In molten YBr_3, the distance and coordination number of the nearest Y^{3+}–Br^- interaction were 2.85 Å and 5.8, respectively. This distance is close to the value of 2.86 Å for molten $HoBr_3$ (Wasse & Salmon, 1999*c*) though there is no data which can be compared directly. The effective ionic size of Ho^{3+}, 0.901 Å (anion coordination

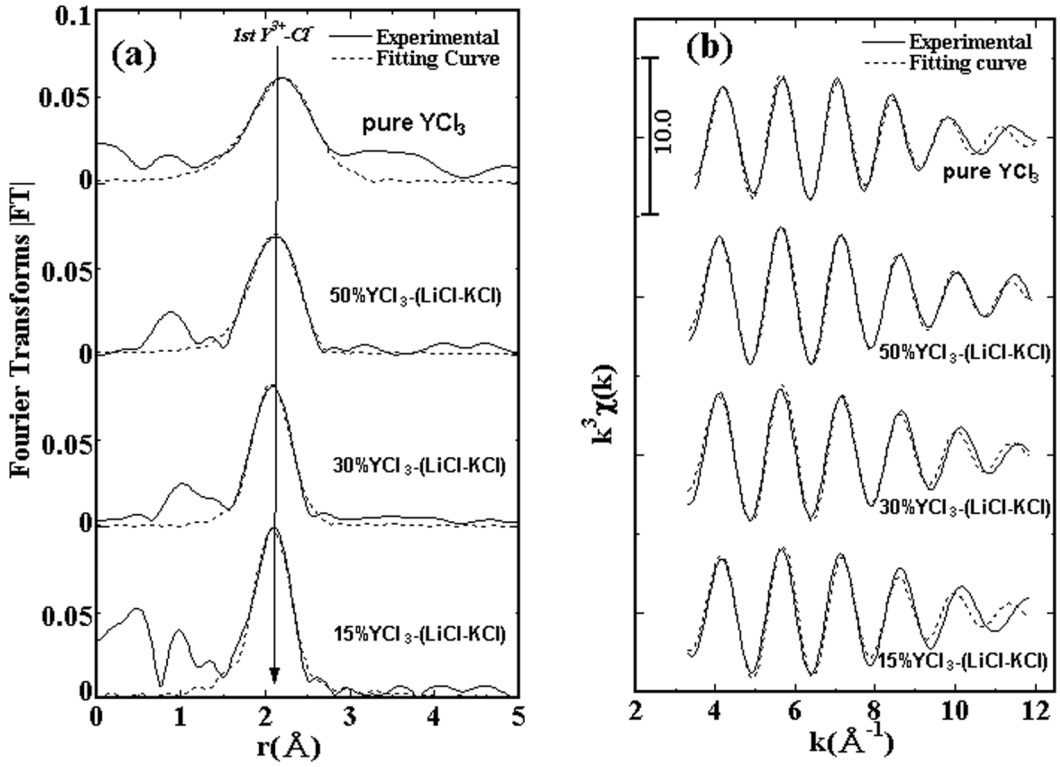

Figure 4
(*a*) Fourier transform of Y *K*-edge EXAFS data and (*b*) the first shell $k^3\chi(k)$ function of molten YCl_3-eutectic LiCl–KCl mixtures.

number = VI) is very close to that of yttrium (0.900 Å) and the crystal structure of YBr_3 is almost the same as that of $HoBr_3$.

In the molten YCl_3, a broad second peak was observed in the range 3 to 4.3 Å. This peak, assigned to the first Y^{3+}–Y^{3+} interaction, is similar to that found in the solid state. The mean distance was evaluated to be 3.9 Å. This value just corresponds to the distance of the Y^{3+}–Y^{3+} interaction in the edge-sharing bridging by Cl^- ions of the two octahedra shown in Fig. 1(*b*). The edge-sharing model has been considered in Raman (Papatheodorou, 1977) and ND (Saboungi *et al.*, 1991) studies of molten YCl_3. Takagi *et al.* (1999) also concluded from an ND experiment that there is an edge-sharing Dy–Cl–Dy cluster in molten $DyCl_3$ that is isostructural in the solid state with YCl_3.

3.2. *Molten YCl_3 with eutectic LiCl–KCl*

Figs. 4(*a*) and 4(*b*) show Fourier transforms without correcting the phase shift and the EXAFS oscillation functions $k^3\chi(k)$ of the first Y^{3+}–Cl^- shell for molten YCl_3–(LiCl–KCl eutectic) mixtures. The EXAFS functions $k^3\chi(k)$ ranging from k = 3.5 to 12 $Å^{-1}$ were used in the Fourier transformation. The first peak corresponding to the nearest Y^{3+}–Cl^- pair became sharper and larger by adding eutectic LiCl–KCl. It can be assigned to a decreasing Debye–Waller factor and/or significant increase in coordination number of the Y^{3+}–Cl^- pair. Drastic changes of the coordination numbers of the halide ions around the metal ion, however, have never been reported in molten salt mixture systems (Tosi *et al.*, 1993). It has been reported that the octahedral coordination $(YCl_6)^{3-}$ is a predominant species and further stabilized by adding KCl (Papatheodorou, 1977). Thus the change is mainly ascribed to the decrease of the Debye–Waller factor. This means that the correlation of the nearest Y^{3+}–Cl^- interaction rises by mixing with the LiCl–KCl eutectic.

The results of the curve fittings in *k*-space are listed in Table 1. The composition dependence of the structural parameters is plotted in Fig. 5 for the distance and the coordination number and in Figs. 6(*a*) and 6(*b*) for the Debye–Waller factor and the third cumulant. The coordination number and the distance for the Y^{3+}–Cl^- pair are almost constant, around 6 and 2.7 Å for each composition. A major change was found in the Debye–Waller factor and the third cumulant *C*3 as shown in Fig. 6(*a*). They decrease significantly by adding

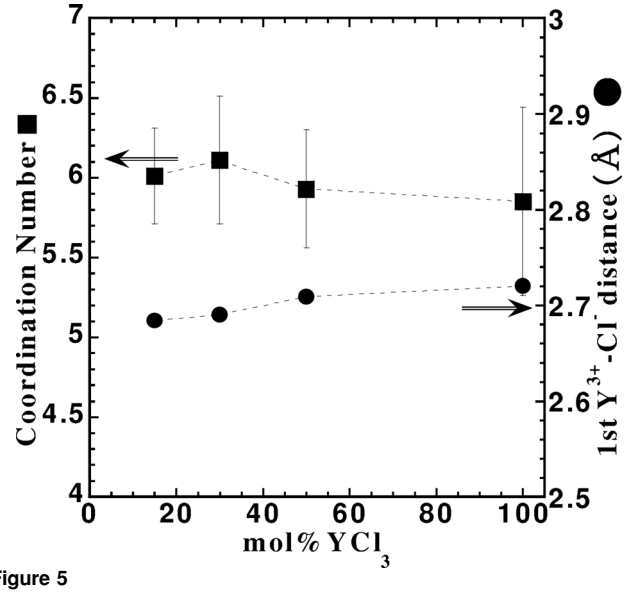

Figure 5
The nearest Y—Cl distance and coordination number of Cl^- around the Y^{3+} ion for molten YCl_3-eutectic LiCl–KCl systems.

Table 3
Structural parameters for the nearest Br^{-}–Y^{3+} pair in solid and molten YBr_3 and molten YBr_3–LiBr system based on the Br *K*-absorption edge.

Coordination number N_Y, interionic distance r_Y, Debye–Waller factor σ^2_{B-Yr}, third and fourth cumulants *C*3 and *C*4.

	N_Y	r_Y (Å)	σ^2_{Br-Y} (Å^2)	*C*3 (10^{-3} Å)	*C*4 (10^{-4} Å)	Residual
Solid YBr_3	2.0 ± 0.1	2.82 ± 0.01	0.0087 ± 0.0004	No anharmonic effects	No anharmonic effects	8.33
Molten YBr_3	2.1 ± 0.3	2.86 ± 0.02	0.0143 ± 0.0007	1.456 ± 0.025	0.269 ± 0.111	15.70
Molten 50%YBr_3	1.5 ± 0.2	2.85 ± 0.02	0.0135 ± 0.0015	1.350 ± 0.032	0.201 ± 0.062	15.23
Molten 30%YBr_3	1.2 ± 0.3	2.85 ± 0.01	0.0134 ± 0.0007	1.167 ± 0.062	0.203 ± 0.114	16.93
Molten 15%YBr_3	1.1 ± 0.2	2.84 ± 0.01	0.0120 ± 0.0002	1.120 ± 0.115	0.095 ± 0.041	10.04

eutectic LiCl–KCl. This suggests that the octahedral coordination is more stable in the mixture with a higher concentration of the alkali chlorides. The difference in the Debye–Waller factor between the pure YCl_3 and the 50% YCl_3 melts is not so large. It is clearly seen that the change in the Debye–Waller factor is noticeable at lower YCl_3 concentrations. This shows that the octahedron is not very stabilized in a YCl_3-rich composition. Papatheodorou (1977) reported that the existence of a highly symmetrical species $(YCl_6)^{3-}$ can be expected for a composition of less than 20% YCl_3 in the molten YCl_3–KCl binary system. The decrease of the third cumulant may be assigned to a low possibility of exchange of the Cl^- ligand between the inside and the outside of the octahedron.

The second broad peak observed in the molten pure YCl_3 disappeared in the mixtures. No significant peak was found beyond the first peak in the mixture melts. This shows that the bridging of the octahedra by the edge-sharing is broken or that an increased structural disorder may be present.

3.3. *Molten YBr_3 with LiBr*

Figs. 7(*a*) and 7(*b*) show Fourier transforms without correcting the phase shift and the EXAFS oscillation functions $k^3\chi(k)$ of the first Y^{3+}–Br^- shell for molten YBr_3–LiBr mixtures. The EXAFS functions $k^3\chi(k)$ ranging from 3.5 to 12 Å^{-1} were used in the Fourier transforms. The first peak corresponding to the nearest Y^{3+}–Br^- interaction is clearly observed in the |FT| function for all mixtures. No significant peaks were found beyond the first peak. Structural parameters from the curve fittings in the *k*-space are listed in Table 2. The coordination number was about 6 for all cases. The nearest Y^{3+}—Br^- distance was also almost constant at 2.85 Å. This suggests that the octahedral coordination $(YBr_6)^{3-}$ is also a predominant species in the mixtures, in agreement with the Raman study (Dracopoulos *et al.*, 1997). The first peak also became sharper by adding LiBr, similar to the case of the molten YCl_3–alkali-chlorides system. Major change was attributed to the Debye–Waller factor, the third and fourth cumulants; the effects are similar to those of the YCl_3–alkali-chlorides. These values decrease as the concentration of the LiBr increases, as shown in Figs. 6(*a*) and 6(*b*).

The raw EXAFS spectra of the Br *K*-edge for the YBr_3–LiBr system are shown in Fig. 8. An unusual change of slope of the baseline was found at around 80–90 eV from the edge. It is based on a double electron excitation of 1*s* 3*d* as observed in molten alkali bromides by Di Cicco *et al.* (1996). Similary, another change was found around 13.65 keV due to a 1*s* 3*p* transition. The three kinds of baselines shown in the figure were defined in the extraction stage of the EXAFS oscillation from the raw data to minimize the effect in the data analysis.

Figs. 9(*a*) and 9(*b*) show Fourier transforms without correcting the phase shift and the EXAFS oscillation functions $k^3\chi(k)$ of the first Br^-–Y^{3+} shell for the molten YCl_3–LiBr mixtures. Structural parameters obtained from the curve-fitting of the Br *K*-edge EXAFS data are listed in Table 3. Three peaks are observed in the |FT| of molten pure YBr_3. The first peak is assigned to the nearest Br^-–Y^{3+} pair. The second peak is mainly due to the Br^-–Br^- interactions inside the octahedron and between the octahedra. The third peak was observed clearly in the pure YBr_3 melt. This is assigned mainly to the Br^-–Br^- and Br^-–Y^{3+} interactions between the octahedra. The nearest Br^-–Li^+ correlation was not observed for the mixtures, because Li is a

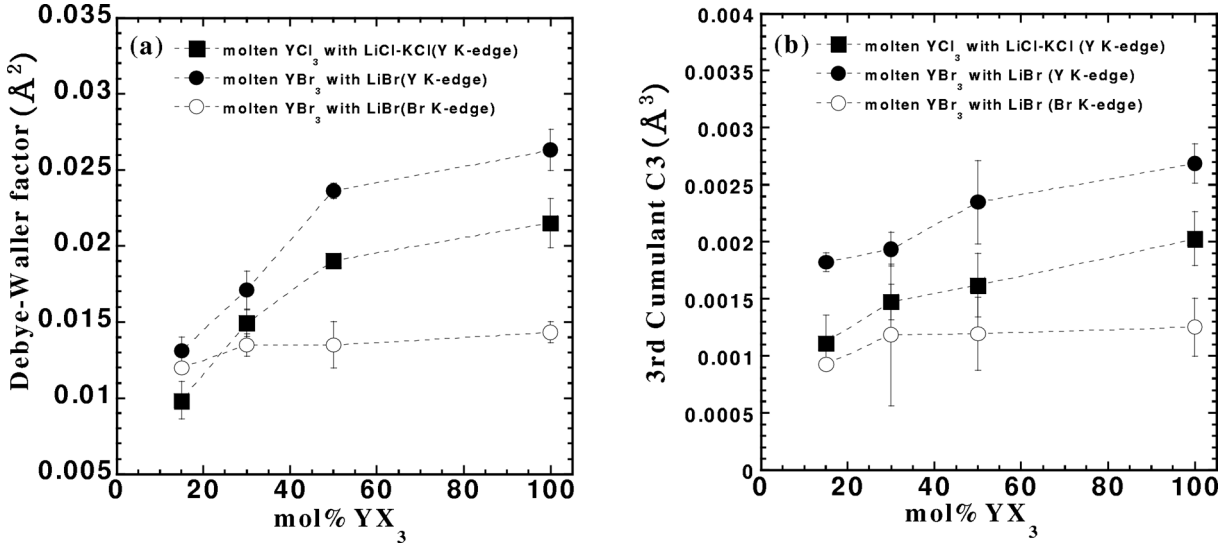

Figure 6
(*a*) Debye–Waller factor σ^2 and (*b*) third cumulant *C*3 of molten YCl_3-eutectic LiCl–KCl mixtures and molten YBr_3–LiBr mixtures.

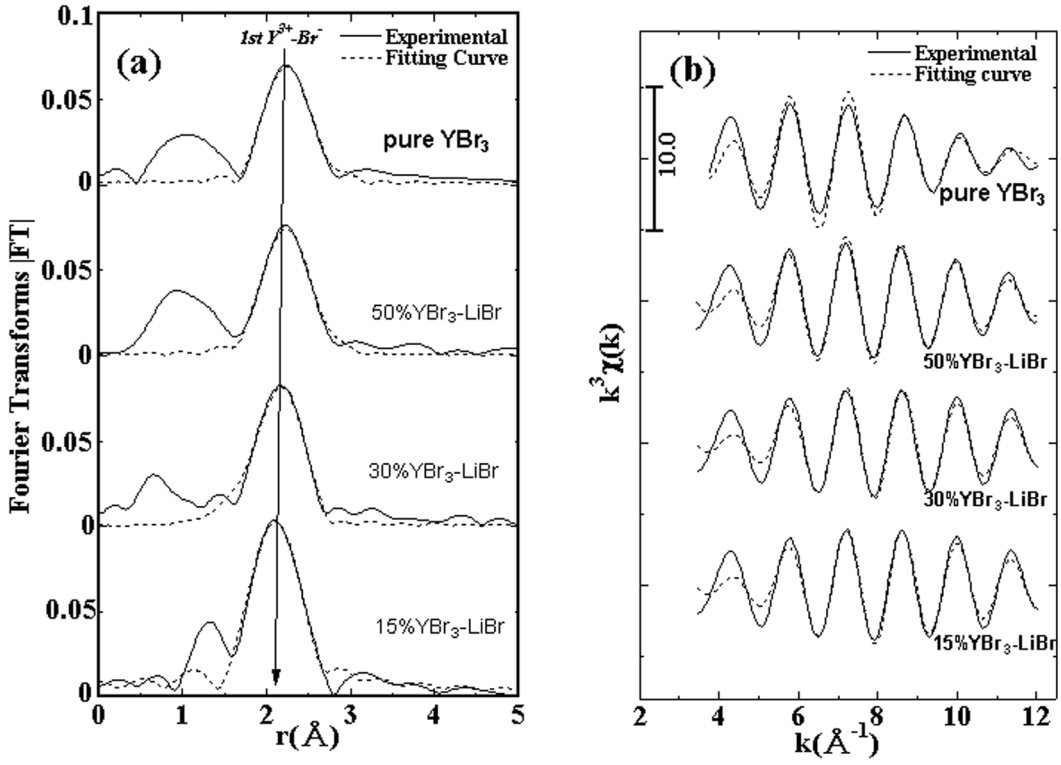

Figure 7
(*a*) Fourier transform of Y *K*-edge EXAFS data and (*b*) the first shell $k^3\chi(k)$ functions of molten YBr_3–LiBr mixtures.

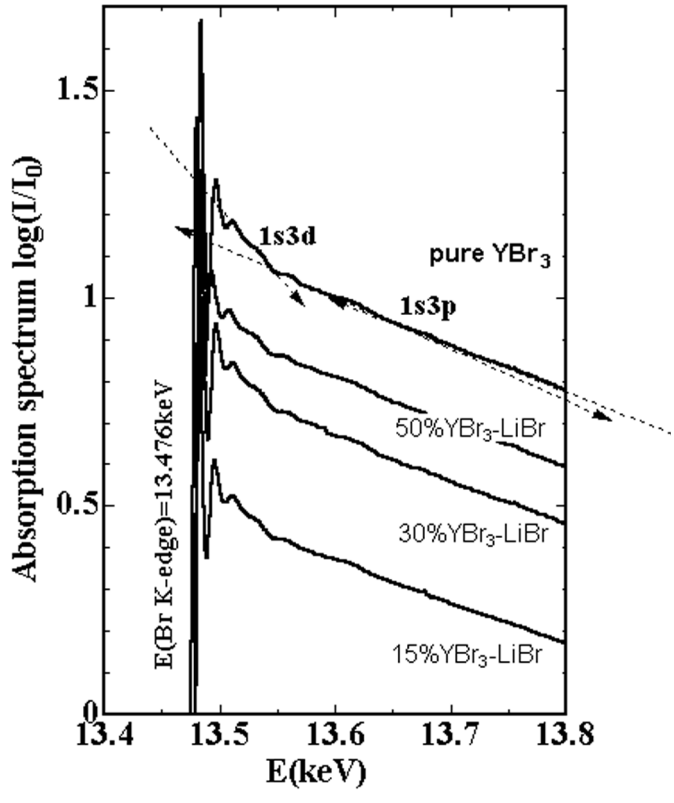

Figure 8
Raw absorption spectra at the Br *K*-edge in molten YBr_3–LiBr mixtures.

weak scatterer. We confirmed that the Br^-–Li^+ correlation was not detected in the XAFS measurement of the solid LiBr. The second and third peaks become unclear by adding LiBr. Contrary to the case of the |FT| of the Y *K*-edge EXAFS (Fig. 7*b*), the first peak became weaker by mixing with LiBr. This suggests that the coordination number decreases and/or the Debye–Waller factor increases. The XAFS function $k^3\chi(k)$ based on the first shell (the first Y^{3+}–Br^- for the Y *K*-edge EXAFS and Br^-–Y^{3+} for the Br *K*-edge EXAFS) derived from Fourier filtering are shown in Figs. 10(*a*) and 10(*b*) for molten pure YBr_3 and the 15% YBr_3–LiBr system. In Fig. 10(*a*) the differences are concentrated in the higher region beyond $k = 8$ Å^{-1}. This deviation can be simply assigned to a change of the Debye–Waller factor as shown in Table 3 and Fig. 6(*a*). On the other hand, differences in the curves of the first Br^-–Y^{3+} shell in Fig. 10(*b*) are mainly observed in the lower k range. The amplitude of the oscillation for the molten pure YBr_3 is clearly larger in the lower k-vector range and smaller beyond $k = 8$ Å^{-1} in comparison with that of the molten 15%YBr_3–LiBr system. No difference was observed in the oscillation phases. It can be deduced that both the coordination number and the Debye–Waller factor changed by mixing with LiBr. From the similarity with Y^{3+}–Br^-, the Debye–Waller factor of the Br^-–Y^{3+} interaction is expected to decrease by mixing with LiBr. As for the results of the fitting, the difference was attributed to a decrease of the coordination number and a decrease of the Debye–Waller factor.

The composition dependence of the structural parameters are summarized in Figs. 11(*a*) and 11(*b*). The coordination number of Y^{3+} around the Br^- ion in molten pure YBr_3 was almost 2. This shows that most Br^- ions inside the octahedron act as corner-sharing bridging ions in the $(YBr_6)^{3-}$ octahedra. The coordination number decreases by adding LiBr. The value for the 50% YBr_3 mixture was about 1.5. It

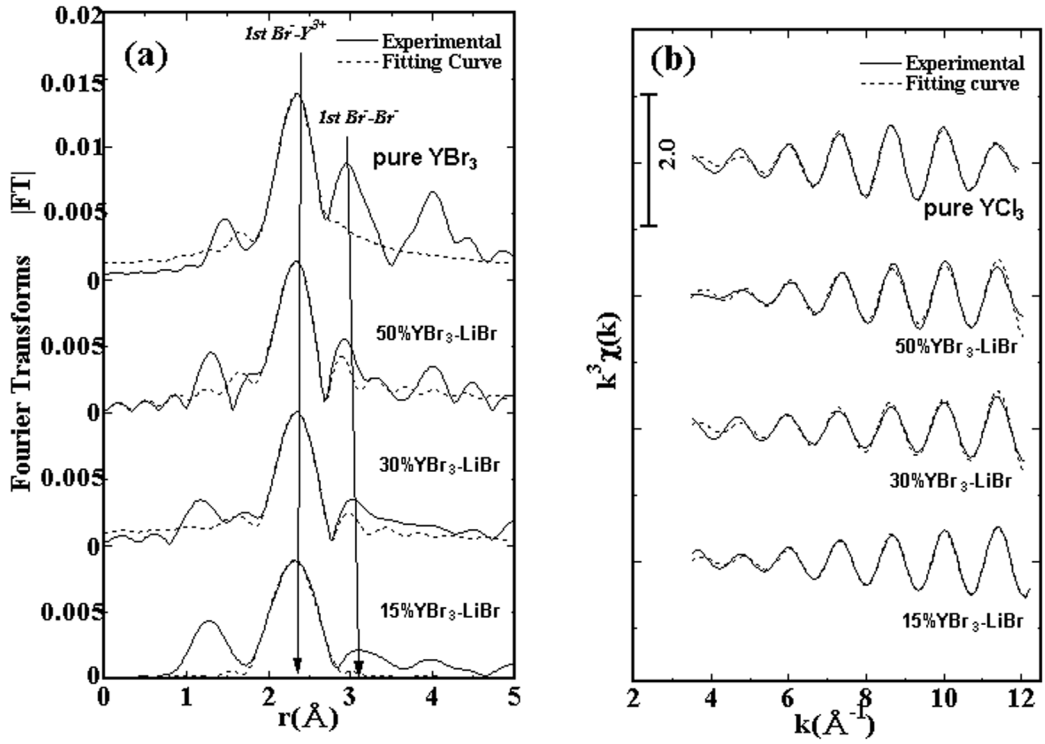

Figure 9
(*a*) Fourier transforms of Br *K*-edge EXAFS data and (*b*) the first shell $k^3\chi(k)$ functions of molten YBr_3–LiBr mixtures.

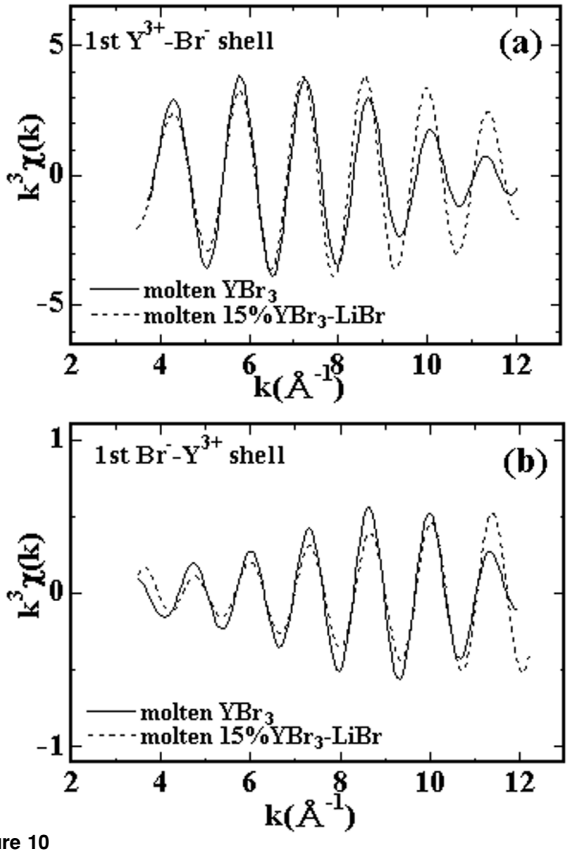

Figure 10
Fourier filterings of the first Y^{3+}–Br^- shell for molten YBr_3 and 15% YBr_3–LiBr mixture.

is roughly estimated that half of the Br^- ions inside the octahedron are not connected to the next octahedron. However, we have to note that this value does not necessarily mean the complete destruction of the network structure. In other words, half of the Br^- ions working as bridging ions may be sufficient to make the loose network structure. The FSDP which is closely associated with the network structure was also observed in ND studies of the trihalide mixtures with alkali halides (Sakurai *et al.*, 1998; Adya *et al.*, 2000). In the 30% and 15% YBr_3 mixtures, the coordination number was about 1 within the error range. This result shows that the bridging ions almost disappeared in mixtures of lower concentrations, *i.e.* less than 30% YBr_3. In addition, it can be concluded that the destruction of the bridging is promoted in the YBr_3 concentration less than 50%.

4. Conclusions

EXAFS measurements of molten YCl_3-eutectic LiCl–KCl and YBr_3–LiBr systems have been performed in order to investigate the local structure and the structural changes caused by mixing. The Y *K*-edge EXAFS data were obtained for the molten YCl_3 and YBr_3 systems. The Br *K*-edge EXAFS were obtained for the molten YBr_3 system. In molten YBr_3 and YCl_3, structural parameters corresponding to the $(MX_6)^{3-}$ octahedral coordination were obtained as the results of the curve fittings. The correlation of the nearest Y^{3+}–Cl^- and Y^{3+}–Br^- interactions become strong by mixing with alkali halides. This corresponds to the stabilization of the octahedron by supplying halide ions as shown by the Raman studies. It is also suggested that the stabilization of the octahedron promotes mainly less than 50% trihalides concentration. In the Br *K*-edge EXAFS analysis of the molten YBr_3–LiBr system, a decrease in the coordination number of Y^{3+} around the Br^- ion was observed by adding LiBr. It is concluded

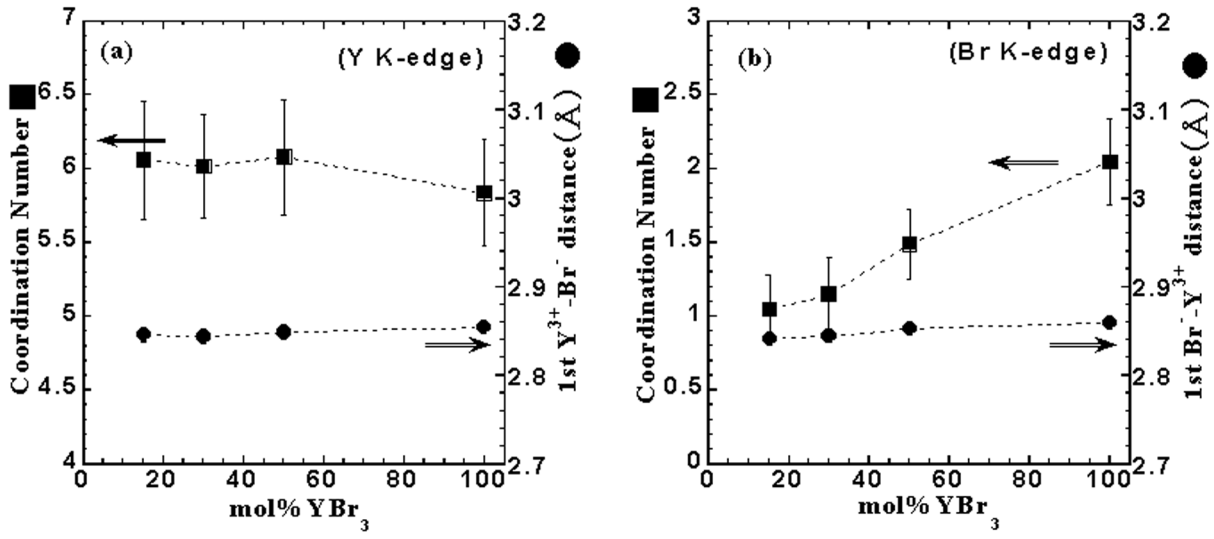

Figure 11
First distance and coordination number of (*a*) Y^{3+}–Br^{-} and (*b*) Br^{-}–Y^{3+} for molten YBr_3–LiBr mixtures.

that destruction of the bridging structure is promoted in the YBr_3 concentration less than 50%.

The authors gratefully acknowledge the interest and encouragement of Dr A. Iwamoto. The authors also thank Professor K. Kobayashi and Dr N. Usami (KEK) for support at the Photon Factory.

References

Ablanov, M., Matsuura, H. & Takagi, R. (1999). *Denki Kagaku*, **67**, 839–842.
Abramo, M. C. & Caccamo, C. (1994). *J. Phys. Condens. Matter*, **6**, 4405–4418.
Adya, A. K., Matsuura, H., Takagi, R., Rycerz, L. & Gaune-Escard, M. (2000). *Proceedings of the 12th International Symposium on Molten Salt*, Honolulu, Hawaii, October 1999, edited by P. C. Trulove, H. C. De Long, G. R. Stafford & S. Deki, pp. 341–355. Pennington, NJ: The Electrochemical Society.
Bunker, G. (1983). *Nucl. Instrum. Methods Phys. Res.* **207**, 437–444.
Di Cicco, A., Minicucci, M. & Filipponi, A. (1997). *Phys. Rev. Lett.* **78**, 460–463.
Di Cicco, A., Rosolen, M. J., Marassi, R., Tossici, R., Filipponi, A. & Rybicki, J. (1996). *J. Phys. Condens. Matter*, **8**, 10779–10797.
Dracopoulos, V., Gilbert, B., Borrensen, B., Photiadis, G. M. & Papatheodorou, G. N. (1997). *J. Chem. Soc. Faraday Trans.* **93**,, 3081–3088.
Eisenberger, P. & Brown, G. S. (1979). *Solid State Commun.* **29**, 481.
Hayashi, H., Okamoto, Y., Ogawa, T., Sato, Y. & Yamamura, T. (1998). *Proceedings of the 5th International Symposium on Molten Salt Chemistry and Technology*, Dresden, Germany, August 1997, edited by H. Wendt, *Molten Salt Forum*, Vols. 5–6, pp. 257–260. Zurich: Trans Tech Publications.
Hutchinson, F., Rowley, A. J., Walters, M. K., Wilson, M., Madden, P. A., Wasse, J. C. & Salmon, P. S. (1999). *J. Chem. Phys.* **111**, 2028–2037.
Mochinaga, J. & Irisawa, K. (1974). *Bull. Chem. Soc. Jpn*, **47**, 364.
Mochinaga, J., Iwadate, Y. & Fukushima, K. (1991). *Mater. Sci. Forum*, **73/75**, 147.
Okamoto, Y., Hayashi, H. & Ogawa, T. (1996). *J. Non-Cryst. Solids*, **205/207**, 139.
Okamoto, Y., Hayashi, H. & Ogawa, T. (1999). *Jpn. J. Appl. Phys.* **38**, 156–159.
Okamoto, Y., Kobayashi, F. & Ogawa, T. (1998). *J. Alloys Comput.* **271/273**, 355–358.
Okamoto, Y., Motohashi, H., Akabori, M. & Ogawa, T. (2000). *Proceedings of the 12th International Symposium on Molten Salt*, Honolulu, Hawaii, October 1999, edited by P. C. Trulove, H. C. De Long, G. R. Stafford & S. Deki, pp. 240–246. Pennington, NJ: The Electrochemical Society.
Okamoto, Y. & Ogawa, T. (1999*a*). *Z. Naturforsch. Teil A*, **54**, 91–94.
Okamoto, Y. & Ogawa, T. (1999*b*). *Z. Naturforsch. Teil A*, **54**, 599–604.
Papatheodorou, G. N. (1975). *Inorg. Nucl. Chem. Lett.* **11**, 483.
Papatheodorou, G. N. (1977). *J. Chem. Phys.* **66**, 2893–2900.
Photiadis, G. M., Borrensen, B. & Papatheodorou, G. N. (1998). *J. Chem. Soc. Faraday Trans.* **94**, 2605–2613.
Ressler, T. (1997). *J. Phys. IV*, **7**(C2), 269–270.
Saboungi, M.-L., Price, D. L., Scamehorn, C. & Tosi, M. P. (1991). *Europhys. Lett.* **15**, 283–288.
Sakurai, M., Takagi, R., Adya, A. K. & Gaune-Escard, M. (1998). *Z. Naturforsch. Teil A*, **53**, 655–658.
Spedding, F. H. & & Danne, A. H. (1960). *Met. Rev.* **5**, 297.
Soldo, Y., Hazemann, J. L., Aberdam, D., Pernot, E., Inui, M., Jal, J. F., Tamura, K., Dupuy-Philon, J. & Raoux, D. (1997). *J. Phys. IV*, **7**(C2), 983–985.
Stern, E. A., Livens, P., Zhang, Z. (1991). *Phys. Rev. B*, 43, 8850–8860.
Takagi, R., Hutchinson, F., Madden, P. A., Adya, A. K. & Gaune-Escard, M. (1999). *J. Phys. Condens. Matter*, **11**, 645–658.
Tosi, M. P., Price, D. L. & & Saboungi, M.-L. (1993). *Annu. Rev. Phys. Chem.* **44**, 173–211.
Van Hung, N., Frahm, R. & Kamitsubo, H. (1996). *J. Phys. Soc. Jpn*, **65**, 3571–3575.
Wasse, J. C. & Salmon, P. S. (1999*a*). *J. Phys. Condens. Matter*, **11**, 1381–1396.
Wasse, J. C. & Salmon, P. S. (1999*b*). *J. Phys. Condens. Matter*, **11**, 9293–9302.
Wasse, J. C. & Salmon, P. S. (1999*c*). *J. Phys. Condens. Matter*, **11**, 2171–2177.
Wasse, J. C., Salmon, P. S. & Delaplane, R. G. (2000). *Physica B*, **276/278**, 433–434.
Xiang-Yun, W., Tian-Zhu, J., Goudiakas, J. & Fuger, J. (1988). *J. Chem. Thermodyn.* **20**, 1195–1202.
Zabinsky, S. I., Rehr, J. J., Ankudinov, A., Albers, R. C. & Eller, M. J. (1995). *Phys. Rev. B*, **52**, 2995–3009.

 Received 16 January 2001 • Accepted 13 September 2001